RESEARCH AND ENGINEERING INNOVATION PROJECTS OF THE NATIONAL ACADEMY OF SCIENCES OF UKRAINE

https://doi.org/10.15407/scine19.06.019

REDKA, M. O. (https://orcid.org/0000-0002-5803-2772),
and KHOROSHYLOV, S. V. (https://orcid.org/0000-0001-7648-4791)
Institute of Technical Mechanics of the National Academy of Sciences of Ukraine
and the State Space Agency of Ukraine,
15, Leshko-Popelya St., Dnipro, 49005, Ukraine,
+380 56 372 0640, office.itm@nas.gov.ua

CONVOLUTIONAL NEURAL NETWORKS FOR DETERMINING THE ION BEAM IMPACT ON A SPACE DEBRIS OBJECT

Introduction. *Space debris is a serious problem that significantly complicates space activity. This problem can be mitigated by active space debris removal. The ion beam shepherd (IBS) concept assumes the contactless removal of a space debris object (SDO) by the plume of an ion thruster (IT). Techniques for determining the force impact from the IT to the SDO are of crucial importance for implementing the IBS concept.*

Problem Statement. *A launcher's upper stage, approximated by a cylinder, is considered an SDO deorbited by the plume of the IT. The SDO can change its orientation and position relative to the shepherd satellite. The shepherd satellite shall be able to determine the force transmitted to the SDO by the IT, using only SDO's images as the input information.*

Purpose. *The study aims to develop a neural net model that can map an SDO image to the force transmitted by an IT plume to this object and estimate the accuracy of such models.*

Material and Methods. *Plasma physics methods are used to obtain ground truth values of the ion beam force. The deep learning methodology is applied to create neural net models.*

Results. *Three different approaches for end-to-end ion force determination have been investigated. The first model uses a single convolutional neural net (CNN). The second model is an ensemble network consisting of four sub-models, and a classifier is used to pick the correct sub-model. The last model is similar to the first one but is trained on all images used for the second model. After training, all three models' accuracy and computational complexity are estimated. These estimates demonstrate the acceptable performance of CNN-based models.*

Conclusions. *This paper demonstrates that CNNs can be used to determine the force impact without knowledge about the SDO position and orientation and significantly faster than the previous methods.*

Keywords: space debris removal, deep learning, ion beam force, convolution neural networks.

Citation: Redka, M. O., and Khoroshylov, S. V. (2023). Convolutional Neural Networks for Determining the Ion Beam Impact on a Space Debris Object. *Sci. innov.*, 19(6), 19—30. https://doi.org/10.15407/scine19.06.019

As a result of human space activity for over 40 years, the near-Earth orbits became polluted with space debris, including different objects, such as launcher stages, non-functioning spacecraft and their parts. The space debris problem makes further space activities more and more complicated [1]. Different approaches to space debris removal have been introduced recently [2—4]. Among those approaches, the ion-beam shepherd (IBS) concept [5] can be selected because it assumes the removal of a space debris object (SDO). The main idea of this concept is to use the momentum from an ion thruster plume to transmit the deorbiting momentum to the SDO. This contactless technique gained interest in the space community because it can provide low-risk SDO removal.

To implement the IBS concept, it is necessary to have an efficient technique to determine the force that transmits the ion thruster (IT) to the SDO because these values are required for mission planning [6] and relative control tasks [7]. The task of ion beam force determination has been addressed in several papers. A model of an IT plume distribution and interaction with an orbital object was presented in [8]. Theoretical principles of modeling an ion beam plume and calculating the transmitted force were proposed in [9]. Since the authors of this work integrated the elementary forces over the SDO surface, the implementation of this approach might be computationally complex. Research [10] presents an attempt to find analytical formulas for the ion beam force. However, such analytical expressions were obtained only for a spherical SDO. A simplified method for calculating the ion beam using a central projection of the SDO is proposed in [11]. Validation results for this method are reported in [12]. Although this method is significantly faster than the original method [9], it still requires significant computational resources and estimates of the SDO's pose. Research [13] uses the idea of central projection and image processing to calculate the ion beam force based on visual images of the SDO.

Research [14] follows the modern tendency to use artificial intelligence methods in space applications [15] and determine the ion beam force utilizing deep learning techniques. According to the results of this paper, the designed model can provide admissible accuracy but requires good estimates of the position and orientation of the SDO. On the other hand, research [16] demonstrates that these features can be obtained from images with the use of convolution neural networks (CNN). The architecture of the CNNs allows for learning complex patterns that are hard to notice during analytical analysis for input visual data with high dimensions. Inspired by this capability of the CNNs, we demonstrate in this research that CNNs can be applied to determine the ion beam force using SDO's images as input. After being trained the CNN-based model does not require any knowledge about the SDO's relative position and orientation. This approach can be used for the objects of different sizes and shapes, which are known.

Using the IBS concept [5], we consider the deorbiting of an SDO from a low Earth orbit. According to this concept, a shepherd satellite (SS) is equipped with an impulse transfer thruster (ITT) and an impulse compensation thruster (ICT). The ion plume from the ITT is pointed towards the SDO and used for transferring the deorbiting momentum. The nozzle of the ICT is pointed in the opposite direction to compensate the reaction force created by the ITT (Fig. 1).

For efficient contactless de-orbiting, the SS has to fly at a sufficiently small distance in front of the SDO of the order of a few SDO diameters. To maintain such a position of the SS for a long period of time, it is necessary to use effective algorithms for controlling its relative motion, for example such as [23]. To implement such algorithms, the ion beam force has to be calculated in orbit with the use of SS computer at each control sampling period. It is problematic to solve this task using traditional force calculation algorithms, since they require a lot of time and computational resources. In addition, such algorithms need information about the SDO's orientation, the detemination of which is also problematic. This research has addressed this problematic situation

ISSN 2409-9066. Sci. innov. 2023. 19 (6)

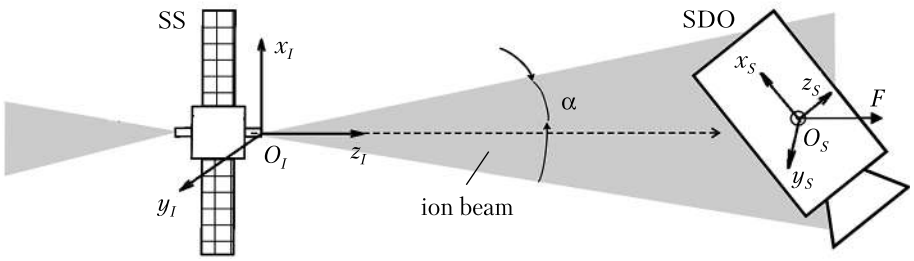

Fig. 1. IBS concept

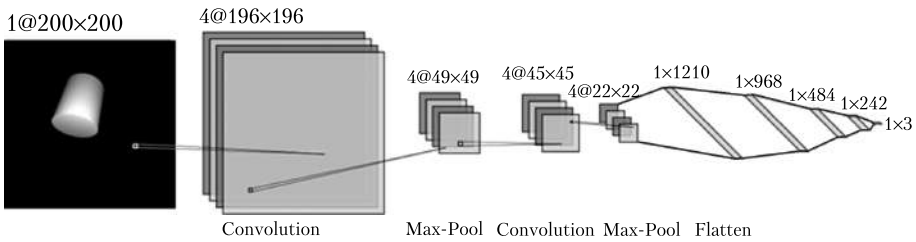

Fig. 2. CNN architecture

by creating a neural network model that uses only camera-acquired images of the SDO as input and allows determining the force faster than by conventional methods.

The study aims to develop a neural net model that can map an SDO image to the force transmitted by an IT plume to this object, and estimate the accuracy of such models.

CNN

An artificial neural network is a system of interconnected artificial neurons [17]. A multilayer neural network consists of input, output and hidden layers of neurons. The most popular multilayer neural networks are feed-forward neural networks with one or more hidden layers in which each neuron of the hidden layer is connected to every neuron of the previous layer. It was proved that such a network with at least one hidden layer could approximate any continuous function of a set of variables; the only condition is the nonlinearity of the activation function in hidden layers [18]. To make a neural network model able to give correct responses for given inputs, it needs to be trained. Supervised learning is the most efficient approach to neural networks. According to this approach, the network weights and biases are optimized to minimize the error between the predicted and ground-truth value of the model output.

In this paper, we propose to use CNNs to determine the force transmitted by the IT plume to an SDO using visual images as input. The CNN is chosen because this architecture is very powerful for the image analysis tasks [19]. CNNs are a subset of feed-forward artificial neural networks and utilize the advantages of using the mathematical operation of convolution, which allows finding complex patterns even in input data of high dimensional, such as images [19]. CNN utilizes the concept of small filters that move along the image to detect features. This approach reduces the number of network parameters that need to be trained because any CNN filter uses the same weights and biases regardless of its position. Yan LeCun et al [20] first demonstrated that the back-propagation technique could be used to train this kind of neural network successfully. CNNs could effectively solve both classification and regression problems by processing black and white or color images.

Figure 2 shows our custom CNN architecture used for this task. The input for the CNN is an SDO's image. The force projections in the IRF are the outputs of the network. The hidden layers include two convolution layers with ReLU activation and two max-pool layers to reduce the dimensions of the features. Four consecutive fully-connected layers with ReLU activations follow the last max-pool layer. The output layer consists of three neurons corresponding to three force projections.

The mean squared error between the predicted and ground truth force values is used as the loss function to train the CNN.

GROUND TRUTH FORCE

The ground truth forces are calculated based on the methodology used for the similar purpose in [14]. According to this methodology the IT plume is a stream of heavy propellant ions (for example, xenon), accelerated to an energy level of several kilo electron-volts. When such a plume acts on a solid body, a force F is applied to it, which is mainly because of the momentum of the plasma ions bombarding the target. Since the plasma density varies in different areas of the plume, the ion beam force can be calculated by integrating the elementary forces dF over the irradiated surface S of the target as

$$F = \int_S dF. \quad (1)$$

Neglecting the effects of plasma ions leaving the target surface, sputtering of its material, and electron pressure, the elementary force transmitted to the elementary area ds of the SDO's surface can be calculated as follows [6]:

$$dF = mnU(-V \cdot U)ds, \quad (2)$$

where m is the ion mass; n is the plasma density; V is the normal unit vector to the elementary area ds; U is the particle velocity vector.

To determine the SDO's relative position and orientation we introduce the following right-handed orthogonal reference frames.

Let us consider ITT-fixed reference frame (IRF) $O_I x_I y_I z_I$, whose origin O_I is located in the center of the beginning of the far region of the ion beam [8]. The axis $O_I z_I$ coincides with the axis of the beam and is directed towards the ITT nozzle. It is assumed that the IT is fixed on the «shepherd» that is oriented in such a way that the axis $O_I z_I$ coincides with the tangent to the orbit and is directed to the target, the axis $O_I y_I$ coincides with the normal to the orbit and is directed in the opposite direction to the Earth, and the axis $O_I x_I$ complements the reference frame to the right-handed one.

The origin of the reference frame that is associated with the SDO (SDF) $O_S x_S y_S z_S$ is located at its geometric center. The direction of the SDF axes coincides with the principle inertia axes of the SDO. The orientation of the SDF axes relative to the IRF is determined by the Euler angles ϕ, ϑ, ψ [12]. The position of the origin of the SDF relative to the IRF is determined by the vector $[x, y, z]^T$.

To determine the plasma density we use the so-called self-similar model of plasma propagation, because it provides a compromise between its complexity and accuracy [8].

Self-similar models are based on the assumption that the nature of ion propagation can be described with the use of a dimensionless similarity function $h(\tilde{z})$. Using this function, we can present the coordinates of the ions as

$$r(z) = r_0\, h(\tilde{z}), = \tilde{z}/R_0,$$

where r, z are the radial and axial coordinates, respectively; R_0, r_0 are the beam radius and radial coordinates of ions at the beginning of the far region ($z - 0$).

In our case the character of plasma distribution can be considered conical and the similarity function can be defined in the following simple form

$$h(\tilde{z}) = 1 + \tilde{z}tan\alpha, \quad (3)$$

where α is the initial divergence half-angle of the IT plume.

With the use of similarity function (3), the plasma density at an arbitrary point of the plume with coordinates r, z can be determined as follows [8]:

$$n_0 = \frac{n_0}{h^2(\tilde{z})} exp\left(-C\frac{\tilde{r}^2}{2h^2(\tilde{z})}\right),\ \tilde{r} = r/R_0, \quad (4)$$

where n_0 is the plasma density at the beginning of the far region of the beam; C is the factor that determines how much of the plasma plume hit a circle of radius R_0 (for example, $C = 6$ corresponds to 95% of the flow hit).

For the considered model, the axial component u_z of the plasma ion velocity can be considered a constant and radial velocity component is determined by the following expression [8]:

$$u_r = u_z \cdot \left(\frac{\tilde{r}}{\tilde{z}}\right). \quad (5)$$

For a specific mission of space debris removal, the IT properties and the shape and size of SDO are known and can be considered constant. In this case, the ion beam force depends only on SDO's the relative position and orientation. Given that and using equations (1)—(5), we have designed a computational function that receives the values of the relative position and orientation of the SDO as an input and outputs ground truth values of the ion beam force in the IRF. Then knowing the information about relative position and orientation for any SDO's synthetic image we can form a training dataset that consists of the input images and corresponding output ion beam forces.

SYSTEM DATA

For all the experiments, we use the following ion thruster parameters: the initial ion thruster radius is $R_0 = 0.0805$ m; the ion mass (xenon) is $m = 2.18 \cdot 10^{-25}$ kg; the initial plasma density is $n_0 = 4.13 \cdot 10^{15}$ m^3; the axial velocity of ions is $u_z = 71580$ m/s; the divergence half-angle is $\alpha = 7$ deg; the nominal thrust of the ITT is 0.031 N.

The upper stage of the Cyclone-3 launch vehicle is considered an SDO that is approximated by a cylinder with a height of 2.6 m and a base diameter of 2.2 m.

DATASETS

The datasets contain the images of the SDO as the input and the corresponding force vector as the output. The ground-truth forces are calculated with the use of the function that is designed based on the methodology from Subsection *Ground truth force*. The inputs for this function are generated randomly with a continuous uniform distribution and variation ranges specifically for each input parameter. Then, we use these input parameters to generate the SDO's synthetic images. The images are rendered with the use of Blender open-source software. A camera focal length of 25 mm and black background are used for rendering grayscale images with a size of 200 × 200 pixels. Some examples of the SDO's images used as inputs for the CNN models are shown in Fig. 3. We did not use any preprocessing techniques for input data, but we normalized outputs using the linear scaling method to have the ground-truth values in a range of [−1.0, 1.0]. Finally, the dataset was split for training and validation with 80% and 20% ratios, respectively.

Three different approaches for the end-to-end training of the CNN have been studied. The first model, called CNN1, uses a single CNN that is trained on the dataset consisting of 10000 SDO images. In this case, the relative position inputs vary in ranges of [−1.0; 1.0] m and [5.0; 9.0] m for x, y and z coordinates, respectively. The input orientation angles ψ, φ, θ vary in a range of [1.57; 1.57] rad. The second model, called CNN2, is an ensemble network. It consists of four sub-models Q1—Q4. Each particular model is trained with its own dataset containing 10000 images. In this case, different models are used to determine the force depending on the relative distances to the

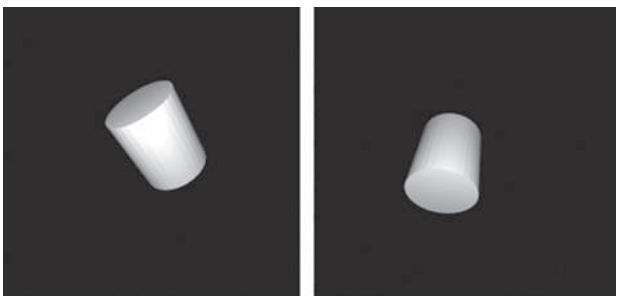

Fig. 3. Examples of input SDO's images

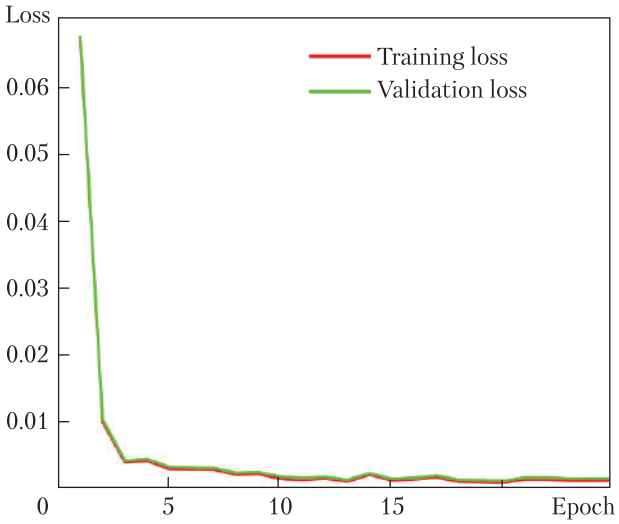

Fig. 4. Loss during training of CNN1 model

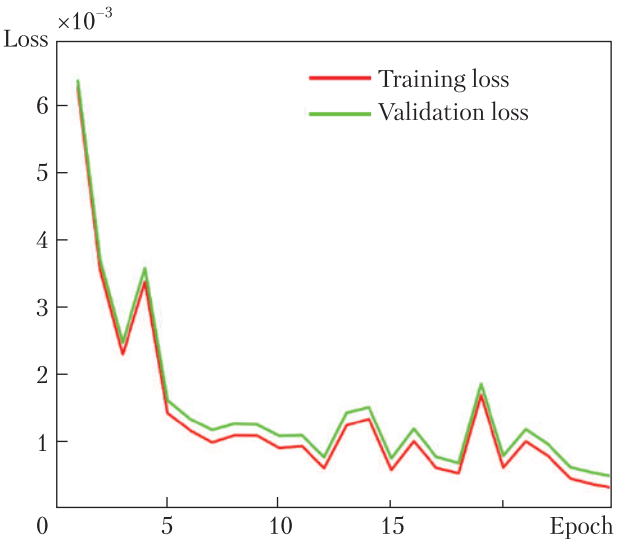

Fig. 5. Loss during training of CNN3 model

SDO, which are given in Table 1. A classifier is used to pick the specific model. To train the classifier, the output regression layer of CNN1 was replaced with a classification layer to perform four-class classification for mapping each classifier output to the specific model. According to this approach, the CNN2 model uses the classifier at first to determine the specific model, and then the specified model performs regression using the same image as the input.

It should be noted that in practice this classification task for CNN2 can be avoided altogether if the spacecraft has other means for determining the relative position of the SDO, such as LIDAR.

The last model, called CNN3, is very similar to the CNN1. However, it is trained on the extended dataset consisting of all images used to train the CNN2 model. Thus, the CNN3 is trained on the dataset containing 40000 images. All three CNN models use the same architecture, showed in Fig. 2.

TRAINING AND VALIDATION

Training, validation and testing of CNN models were implemented with the use of Python 3.9 programming language and PyTorch open-source machine learning framework. All models are trained on a desktop PC with Intel 10th generation processor with 8 cores and 16 threads and Nvidia GPU with Ampere architecture, utilizing higher memory bandwidth to speed up the training process [21]. CNN models were initialized by the Xavier method [22]. The parameters of the Adam optimizer are selected as follows: the gradient damping factor is 0.9; the attenuation coeffi-

Table 1. **Input Ranges for Ensemble Sub-Models**

Sub-model	Input range					
	x	y	z	ψ	φ	θ
Q1	[−1; 0]	[0; 1]	[5; 9]	[−1.57; 1.57]	[−1.57; 1.57]	[−1.57; 1.57]
Q2	[0; 1]	[0; 1]	[5; 9]	[−1.57; 1.57]	[−1.57; 1.57]	[−1.57; 1.57]
Q3	[0; 1]	[−1; 0]	[5; 9]	[−1.57; 1.57]	[−1.57; 1.57]	[−1.57; 1.57]
Q4	[−1; 0]	[−1; 0]	[5; 9]	[−1.57; 1.57]	[−1.57; 1.57]	[−1.57; 1.57]

ISSN 2409-9066. Sci. innov. 2023. 19 (6)

cient of the squared gradient is 0.999; the small constant is $7.0 \cdot 10^{-7}$. Each CNN is trained on 25 epochs with a learning rate of 0.001 and a mini-batch size of 256.

Computation time was also considered a performance metric. In order to determine it, we wrapped the code that performs neural network inference into Python code that measures execution time in milliseconds for each computational case during testing. The traditional solution has been used as a standalone Python package with a callable function; the execution time was measured the same way as for the neural networks. All time measuring was performed on the same PC with the same hardware.

TRAINING

Figure 4 shows the plots of the training and validation losses for the CNN1 model. The training of the CNN1 model for 25 epochs lasted 501.172 s and finished with training and validation losses of $6.88 \cdot 10^{-4}$ and $1.26 \cdot 10^{-3}$, respectively.

Each particular sub-model of the ensemble model CNN2 is trained independently with the use of specific dataset. The training results for sub-models used to determine the force are given in Table 2.

Figure 5 shows training and validation losses for the CNN3 model. The average training and validation losses for CNN3 are $7.54 \cdot 10^{-4}$ and $8.53 \cdot 10^{-4}$, respectively.

The CNN3 model required 2045.6 s to train. This is almost three times longer than any other regression models we trained during this research because a significantly bigger training dataset is used for training the CNN3.

TESTING

We tested our trained CNN models considering different positions and orientations of the SDO relative to the ITT. The parameters for 18 testing cases are summarized in Table 3. The parameters marked as "*" vary within the considered ranges with a fixed step of 0.001. The fixed parameters of the first 6 cases have nominal values. The normalized error vector are defined in the following way: $\Delta F = F_R - F_P$, where F_R is the normalized reference force; F_P is the normalized predicted force.

Figures 6—8 show normalized errors obtained for case 3 with the use of CNN1, CNN2, and CNN3 models, respectively. The variable parameter and normalized error for each of the outputs of the CNNs vary along the ordinate and abscissa axes, respectively.

Table 2. **Average Loss for CNN2 Sub-Models**

Sub-model	Average loss	
	Training	Validation
Q1	$4.4 \cdot 10^{-4}$	$4.9 \cdot 10^{-4}$
Q2	$9.8 \cdot 10^{-4}$	$1.19 \cdot 10^{-3}$
Q3	$5.5 \cdot 10^{-4}$	$6.4 \cdot 10^{-4}$
Q4	$6.0 \cdot 10^{-4}$	$7.2 \cdot 10^{-4}$

Table 3. **SDO's Position and Orientation**

Case	Position			Orientation		
	x, m	y, m	z, m	ψ, rad	φ, rad	θ, rad
1	*	0	7	0	0	0
2	0	*	7	0	0	0
3	0	0	*	0	0	0
4	0	0	7	*	0	0
5	0	0	7	0	*	0
6	0	0	7	0	0	*
7	*	1	9	1.507	1.507	1.507
8	1	*	9	1.507	1.507	1.507
9	1	1	*	1.507	1.507	1.507
10	1	1	9	*	1.507	1.507
11	1	1	9	1.507	*	1.507
12	1	1	9	1.507	1.507	*
13	*	1	9	−1.507	−1.507	−1.507
14	1	*	9	−1.507	−1.507	−1.507
15	1	1	*	−1.507	−1.507	−1.507
16	1	1	9	*	−1.507	−1.507
17	1	1	9	−1.507	*	−1.507
18	1	1	9	−1.507	−1.507	*

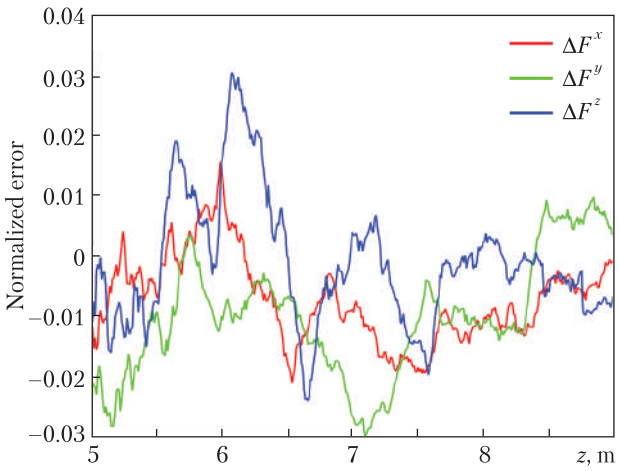

Fig. 6. Normalized errors of CNN1 for case 3

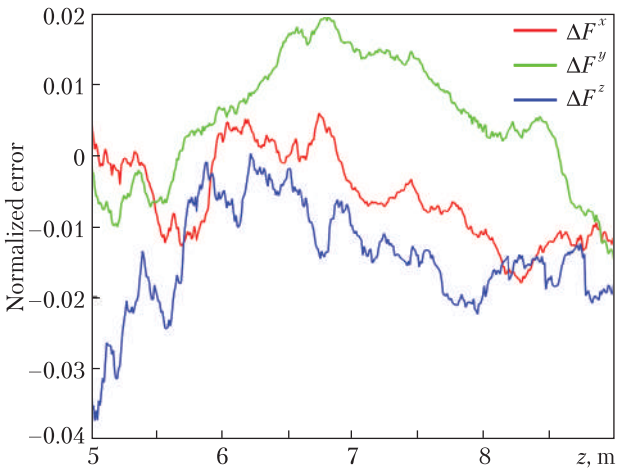

Fig. 7. Normalized errors of CNN2 for case 3

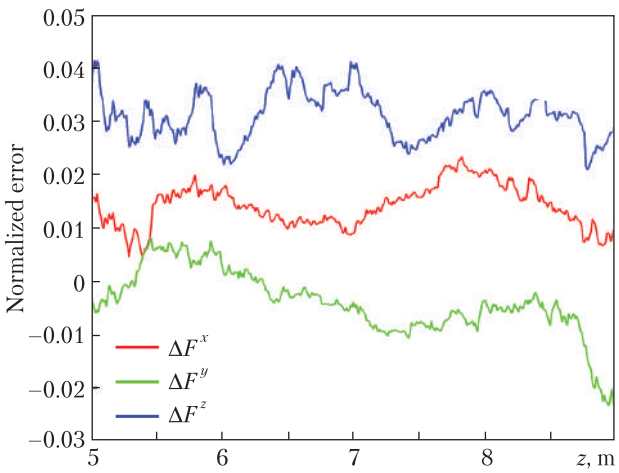

Fig. 8. Normalized errors of CNN3 for case 3

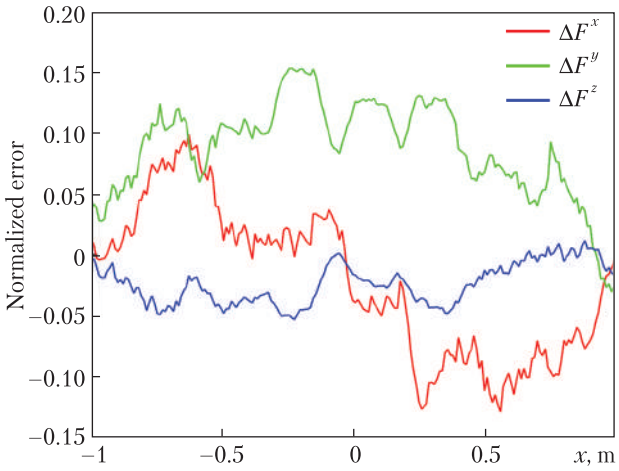

Fig. 9. Normalized errors of CNN1 for case 13

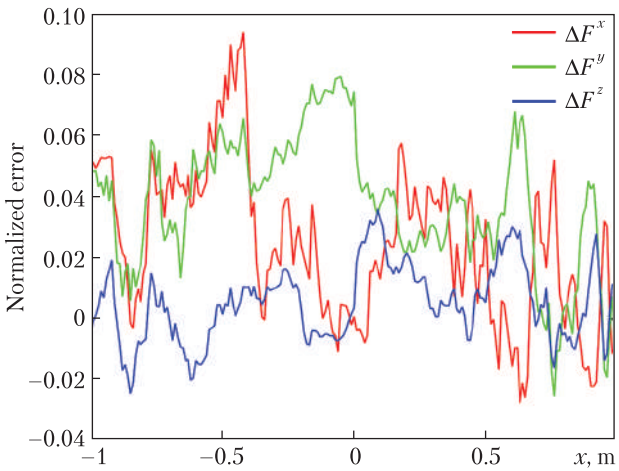

Fig. 10. Normalized errors of CNN2 for case 13

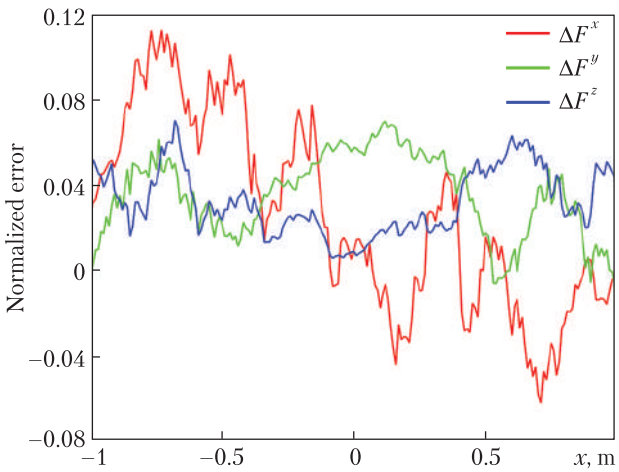

Fig. 11. Normalized errors of CNN3 for test case 13

Figures 9—11 show the results of testing of models using test case 13. It has non-nominal constant parameters, and the parameter that varies is the relative distance using x axis.

Table 4 presents the maximum normalized errors for three CNN models and all test cases. As can be seen from this table, CNN3 is the most accurate model, with an average normalized error of 7.689%. All models demonstrated the best accuracy in case 4 with normalized errors of 2.863% ($1.821 \cdot 10^{-5}$ N), 1.555% ($9.888 \cdot 10^{-6}$ N) and 4.131% ($1.326 \cdot 10^{-3}$ N) for the CNN1, CNN2, CNN3, respectively.

Testing case 15 is the worst for the CNN1 model, where a relative error of 27.492% and an absolute error of $1.754 \cdot 10^{-4}$ N were registered. CNN2 demonstrates the worst accuracy in testing case 14 with a relative error of 16.889% and an absolute error of $1.070 \cdot 10^{-4}$. For the CNN3 model, a maximum relative error of 15.323% and an absolute error of $9.76 \cdot 10^{-5}$ N are the less accurate results, which is reported in case 15. In this regard, CNN3 is similar to CNN1.

Although some relative errors may seem pretty significant, their impact on the SDO is minimal. For example, a relative error of 27.492% for CNN1 corresponds to an absolute error of $1.754 \cdot 10^{-4}$ N that is only 0.5% from the nominal thrust of the ITT.

Due to the SDO deorbiting purpose the ion beam forces in x and y directions are significantly smaller than those in z direction and the absolute errors also keep this tendency. The errors in z direction go up with the number of ions missing the target, which depends on SDO's relative position and orientation in a complex way.

Another conclusion that can be drawn from the testing results is that the ion force prediction's

Table 4. **Maximum Errors**

Case	Maximum normalized error, %			Maximum absolute error, N		
	CNN1	CNN2	CNN3	CNN1	CNN2	CNN3
1	18.751	11.195	7.686	$1.192 \cdot 10^{-4}$	$7.131 \cdot 10^{-5}$	$4.896 \cdot 10^{-5}$
2	18.855	9.607	9.558	$1.203 \cdot 10^{-4}$	$6.101 \cdot 10^{-5}$	$6.088 \cdot 10^{-5}$
3	3.01	3.738	4.132	$9.665 \cdot 10^{-4}$	$1.200 \cdot 10^{-3}$	$1.327 \cdot 10^{-3}$
4	2.863	1.555	4.131	$1.821 \cdot 10^{-5}$	$9.888 \cdot 10^{-6}$	$1.326 \cdot 10^{-3}$
5	3.846	3.525	5.486	$1.235 \cdot 10^{-3}$	$1.132 \cdot 10^{-3}$	$1.761 \cdot 10^{-3}$
6	3.999	3.869	4.411	$2.551 \cdot 10^{-5}$	$1.242 \cdot 10^{-3}$	$1.416 \cdot 10^{-3}$
7	15.26	9.372	11.259	$9.705 \cdot 10^{-5}$	$5.970 \cdot 10^{-5}$	$7.172 \cdot 10^{-5}$
8	13.976	16.879	7.085	$8.889 \cdot 10^{-5}$	$1.074 \cdot 10^{-4}$	$4.513 \cdot 10^{-5}$
9	27.192	9.677	15.321	$1.750 \cdot 10^{-4}$	$6.164 \cdot 10^{-5}$	$9.761 \cdot 10^{-5}$
10	4.277	2.865	3.785	$2.720 \cdot 10^{-5}$	$1.825 \cdot 10^{-5}$	$1.215 \cdot 10^{-3}$
11	14.005	13.022	10.268	$8.935 \cdot 10^{-5}$	$8.295 \cdot 10^{-5}$	$6.541 \cdot 10^{-5}$
12	4.277	2.865	3.785	$2.720 \cdot 10^{-5}$	$1.825 \cdot 10^{-5}$	$1.215 \cdot 10^{-3}$
13	15.26	9.372	11.259	$9.705 \cdot 10^{-5}$	$5.970 \cdot 10^{-5}$	$7.172 \cdot 10^{-5}$
14	13.944	16.889	7.085	$8.868 \cdot 10^{-5}$	$1.074 \cdot 10^{-4}$	$4.513 \cdot 10^{-5}$
15	27.492	9.677	15.323	$1.754 \cdot 10^{-4}$	$6.164 \cdot 10^{-5}$	$9.760 \cdot 10^{-5}$
16	4.271	2.843	3.782	$2.716 \cdot 10^{-5}$	$1.811 \cdot 10^{-5}$	$1.214 \cdot 10^{-3}$
17	14.235	12.99	10.255	$9.082 \cdot 10^{-5}$	$8.275 \cdot 10^{-5}$	$6.533 \cdot 10^{-5}$
18	4.283	2.865	3.785	$2.724 \cdot 10^{-5}$	$1.825 \cdot 10^{-5}$	$1.215 \cdot 10^{-3}$
Avg	11.655	7.934	7.689	$1.942 \cdot 10^{-4}$	$2.452 \cdot 10^{-4}$	$6.311 \cdot 10^{-4}$

Table 5. **Computation Time**

Time, s			
Ground truth	CNN1	CNN2	CNN3
19.99	8.49	8.50	8.65

accuracy goes up with the size of the dataset used for training.

COMPUTATION TIME

The computation time required to determine the ion beam force by the ground truth function (traditional method) and CNN models is presented in Table 5.

This table shows that every trained CNN model can determine the ion beam force significantly faster than the traditional method. Although there is little difference in time performance between the CNN models, they are all at least twice as fast as the conventional method. These results demonstrate that the CNN model is an alternative technique for determining the ion beam force, providing admissible accuracy and a shorter computation time than the conventional approach.

The relative dynamics of the SS-SDO system is quite slow [7]. According to our estimates, the SS relative motion can be controlled with a sampling period up to 10 s. This time is sufficient to determine the force by our method.

This paper demonstrates how CNNs can be used to determine the force impact of the IT plume on SDO. The CNN models can determine the force impact without prior information about SDO's relative position and orientation using only the SDO's images as input. Moreover, CNNs make it possible to obtain the results significantly faster in comparison with the methods used before. Although the CNN models turn out less accurate than the conventional method, their errors are insignificant for practical applications. In addition, the accuracy issue can be tackled with the use of a more extensive dataset during the training phase. All these features allow us to state that the CNN model is a promising technique for both spacecraft onboard algorithms and the simulation of contactless space debris removal missions.

In the future, it is planned to study the CNN models with the use of more realistic SDO's images obtained in space environment.

REFERENCES

1. Liou, J.-C., Anilkumar, A. K., Virgili, B., Hanada, Toshiya, Krag, H., Lewis, H., Raj, M., Rao, M., Rossi, A., Sharma, R. (2013). "Stability of the future LEO environment — an IADC comparison study". *Proc. of the 6th European Conference on Space Debris* (*22—25 April, 2013, Darmstadt*). URL: https://conference.sdo.esoc.esa.int/proceedings/sdc6/paper/199 (Last accessed: 28.03.2022).
2. Hakima, H., Reza Emami, M. (2018). Assessment of active methods for removal of LEO debris. *Acta Astronautica*, 144, 225—243. https://doi.org/10.1016/j.actaastro.2017.12.036
3. Dron, N. M., Golubek, A. V., Dreus, A. Yu., Dubovik, L. G. (2019). Prospects for the use of the combined method for deorbiting of large-scale space debris from near-Earth space. *Space Science and Technology*, 25(6), 61—69. https://doi.org/10.15407/knit2019.06.061
4. Lapkhanov, E., Khoroshylov, S. (2019). Development of the aeromagnetic space debris deorbiting system. *Eastern-European Journal of Enterprise Technologies*, 5(5 (101)), 30—37. https://doi.org/10.15587/1729-4061.2019.179382
5. Bombardelli, C., Peláez, J. (2011). Ion Beam Shepherd for Contactless Space Debris Removal. *J. Guid. Control Dyn.*, 34(3), 916—920. https://doi.org/10.2514/1.51832
6. Urrutxua, H., Bombardelli, C., Hedo, J. M. (2019). A preliminary design procedure for an ion-beam shepherd mission. *Aerospace Science and Technology*, 88, 421—435. https://doi.org/10.1016/j.ast.2019.03.038
7. Khoroshylov, S. (2018). Relative motion control system of SC for contactless space debris removal. *Sci. innov.*, 14(4), 5—16. https://doi.org/10.15407/scin14.04.005
8. Cichocki, F., Merino, M., Ahedo, E. (2015). Collisionless Plasma thruster plume expansion model. *Plasma Sources Science and Technology*, 24(3), 83—95. https://doi.org/10.1088/0963-0252/24/3/035006

9. Bombardelli, C., Urrutxua, H., Merino, M., Ahedo, E., Pelaez, J. (2012). Relative dynamics and control of an ion beam shepherd satellite. *Spaceflight mechanics*, 143, 2145—2158.
10. Bombardelli, C., Urrutxua, H., Merino, M., Ahedo, E., Pelaez, J., Olympio, J. (2011). Dynamics of ion-beam-propelled space debris. *22nd International Symposium on Space Flight Dynamics (February 28 — March 4, 2011, Sao Jose dos Campos, Brasil)*. 1—13.
11. Alpatov, A., Cichocki, F., Fokov, A., Khoroshylov, S., Merino, M., Zakrzhevskii, A. (2016). Determination of the force transmitted by an ion thruster plasma plume to an orbital object. *Acta Astronaut*, 119(2—3), 241—251. https://doi.org/10.1016/j.actaastro.2015.11.020
12. Fokov, A. A., Khoroshilov, S. V. (2016). Validation of simplified method for calculation of transmitted force from plume of electric thruster to orbital object. *Aviatsionno-kosmicheskaya tekhnika i tekhnologiya*, 2, 55—66.
13. Alpatov, A., Cichocki, F., Fokov, A., Khoroshylov, S., Merino, M., Zakrzhevskii, A. (2015). Algorithm for Determination of Force Transmitted by Plume of Ion Thruster to Orbital Object Using Photo Camera. *Proceedings of the 66th International Astronautical Congress, IAC* (*12—16 October, 2015, Jerusalem, Israel*). 2239—2247.
14. Redka, M. O., Khoroshylov, S. V. (2022). Determination of the force impact of an ion thruster plume on an orbital object via deep learning. *Space Science and Technology*, 28 (5), 15—26. https://doi.org/10.15407/knit2022.05.015
15. Khoroshylov, S. V., Redka, M. O. (2021). Deep learning for space guidance, navigation, and control. *Space Science and Technology*, 27 (6), 38—52. https://doi.org/10.15407/knit2021.06.038
16. Koizumi, S., Kikuya, Y., Sasaki, K., Masuda, Y., Iwasaki, Y., Watanabe, K., Yatsu, Y., Matunaga, S. (2018). Development of attitude sensor using deep learning. *AIAA/USU Conference on Small Satellites, AIAA* (*4—9 August, 2018, Utah, USA*). Session 7: Advanced Concepts II.
17. Haykin, S. (1998). *Neural Networks: A Comprehensive Foundation*. Prentice Hall.
18. Hornik, K. (1991). Approximation capabilities of multilayer feedforward networks. *Neural Networks*, 4(2), 251—257.
19. Venkatesan, R., Li, B. (2017). *Convolutional Neural Networks in Visual Computing: A Concise Guide*. CRC Press.
20. LeCun, Y., Boser, B., Denker, J. S., Henderson, D., Howard, R. E., Hubbard, W., Jackel, L. D. *Backpropagation Applied to Handwritten Zip Code Recognition*. AT&T Bell Laboratories.
21. Steinkraus, D., Simard, P., Buck I., (2005). Using GPUs for Machine Learning Algorithms. *12th International Conference on Document Analysis and Recognition* (*ICDAR 2005*) (*25—28 August 2013, Washington, DC, USA*). 1115—1119. https://doi.org/10.1109/ICDAR.2005.251
22. Glorot, X., Bengio, Y. (2010). Understanding the Difficulty of Training Deep Feedforward Neural Networks. *Proceedings of the Thirteenth International Conference on Artificial Intelligence and Statistics. Proceedings of Machine Learning Research* (*13—15 May, 2010 Sardinia, Italy*). 9, 249—256.
23. Khoroshylov, S. (2019). Out-of-plane relative control of an ion beam shepherd satellite using yaw attitude deviations. *Acta Astronaut*., 164, 254—261. https://doi.org/10.1016/j.actaastro.2019.08.016

Received 10.02.2023
Revised 08.06.2023
Accepted 21.06.2023

М.О. Редька (https://orcid.org/0000-0002-5803-2772),
С.В. Хорошилов (https://orcid.org/0000-0001-7648-4791)

Інститут технічної механіки Національної академії наук України
і Державного космічного агентства України,
вул. Лешко-Попеля, 15, Дніпро, Україна, 49005,
+380 56 372 0640, office.itm@nas.gov

ЗГОРТКОВІ НЕЙРОННІ МЕРЕЖІ ДЛЯ ВИЗНАЧЕННЯ ВПЛИВУ ІОННОГО ПРОМЕНЯ НА ОБ'ЄКТ КОСМІЧНОГО СМІТТЯ

Вступ. Сміття на навколоземних орбітах є серйозною проблемою, що заважає подальшій діяльності людини у космосі, яку можна частково вирішити через активне видалення об'єктів космічного сміття (ОКС). Пастух з іонним променем (ПІП) — це концепція, яка дозволяє безконтактно видаляти ОКС за допомогою факелу електрореактивного двигуна (ЕРД). Для реалізації концепції видалення космічного сміття ПІП потрібні методи визначення сили, що передається від ЕРД до ОКС.

Проблематика. Як ОКС розглядається верхня ступінь ракети-носія, що апроксимована за допомогою циліндра. Цей об'єкт підлягає видаленню з орбіти за допомогою факелу ЕРД космічного апарату-пастуха (КА-П). ОКС може змінювати орієнтацію та положення відносно КА-П. КА-П необхідно визначити силу, що передається ОКС від ЕРД, використовуючи тільки зображення ОКС як вхідну інформацію.

Мета. Створення нейромережевої моделі, яка за зображенням ОКС визначає силу, що передається факелом ЕРД цьому об'єкту, та визначення точності таких моделей.

Матеріали й методи. Методи фізики плазми використано для отримання еталонних значень сили іонного променю, глибинне навчання — для створення нейромережевих моделей.

Результати. Досліджено три різних підходи для визначення сили променя ЕРД. Перша модель використовує єдину згорткову нейронну мережу (ЗНМ). Друга модель є ансамблевою мережею і використовує чотири допоміжні моделі та класифікатор, що визначає необхідну допоміжну модель. Третя модель має таку саму архітектуру, як і перша, але для її навчання застосовано усі зображення, які використано для навчання другої моделі. Після навчання для всіх моделей визначено точність та швидкість визначення сили. Отримано прийнятні показники визначення сили за допомогою моделей, що використовують ЗНМ.

Висновки. Показано, що ЗНМ можуть бути застосовані для визначення силового впливу ЕРД на ОКС без попередньої інформації щодо орієнтації та положення ОКС та є суттєво швидшими за традиційні методи.

Ключові слова: видалення космічного сміття, глибинне навчання, силовий вплив електро-реактивного двигуна, згорткові нейронні мережі.